



Cite this: *New J. Chem.*, 2022, 46, 21401

Preparation and bioevaluation of [^{99m}Tc]Tc-labeled A7R and ^DA7R for SPECT imaging of triple-negative breast cancer

Hongxing Su,^a Lingzhou Zhao,^a Buhui Yu,^a Huahui Zeng,^b Jiqin Yang,^{*c} Meilin Zhu^{*d} and Jinhua Zhao^{ib *a}

Novel strategies for diagnosing triple-negative breast cancer (TNBC) are essential for effective clinical treatment. Vascular endothelial growth factor receptor 2 (VEGFR2) and neuropilin-1 (NRP-1) are potential targets for tumor imaging agents. We designed and synthesized [^{99m}Tc]Tc-labeled heptapeptide (A7R) and its D-type peptide (^DA7R) with high affinity and specificity for VEGFR2 and NRP-1 as novel single-photon emission computed tomography (SPECT) probes for TNBC imaging. The specificities of A7R and ^DA7R were first evaluated *in vitro* using flow cytometry and confocal microscopy and *ex vivo* using fluorescence imaging. Subsequently, A7R and ^DA7R were labeled with [^{99m}Tc]Tc through 6-hydrazino nicotinamide (HYNIC), and their radiochemical purities (RCPs) and stability *in vitro* were assessed. The imaging performance and biodistribution of [^{99m}Tc]Tc-HYNIC-A7R and [^{99m}Tc]Tc-HYNIC-^DA7R were evaluated in TNBC mouse models. A7R and ^DA7R exhibited good TNBC cell-targeting abilities and were readily labeled with [^{99m}Tc]Tc through HYNIC. Both [^{99m}Tc]Tc-HYNIC-A7R and [^{99m}Tc]Tc-HYNIC-^DA7R had high RCPs and stability *in vitro*, and their accumulation in tumor tissues in the TNBC models was evident, with fast blood clearance and favorable biodistribution. More importantly, [^{99m}Tc]Tc-HYNIC-^DA7R showed better tumor-to-muscle ratios and lower renal uptake than [^{99m}Tc]Tc-HYNIC-A7R. These results suggest that both [^{99m}Tc]Tc-HYNIC-^DA7R and [^{99m}Tc]Tc-HYNIC-A7R have substantial potential as probes for targeted SPECT imaging of TNBC, and the former may be considered for future clinical translation owing to its superior tumor imaging performance.

Received 19th August 2022,
Accepted 24th October 2022

DOI: 10.1039/d2nj04136g

rsc.li/njc

Introduction

Breast cancer accounts for 11.7% of all cancer diagnoses and has surpassed lung cancer as the most common cancer among females.¹ Triple-negative breast cancer (TNBC), which does not express the estrogen or progesterone receptor, or the human epidermal growth factor receptor 2, is considerably different from other breast cancer subtypes in molecular genetics, histopathology, and clinical features.^{2–4} Because TNBC has a high mortality rate, early and accurate detection to obtain more effective clinical treatment is needed.^{2,5} However, current

diagnostic methods, including ultrasonography, mammography, and magnetic resonance imaging, cannot specifically detect TNBC.⁶ Therefore, exploring novel strategies to more accurately and rapidly diagnose TNBC is of great significance to clinicians.

Angiogenesis is a crucial step in tumor growth and metastasis.⁷ The interaction among vascular endothelial growth factor-165, vascular endothelial growth factor receptor 2 (VEGFR2) and neuropilin-1 (NRP-1) promotes angiogenesis and vasculature development.^{8–12} NRP-1 also promotes tumor metastasis and is significantly upregulated in TNBC compared to other breast cancer subtypes.^{13–15} Therefore, VEGFR2 and NRP-1 have been identified as targets for the development of various imaging agents for tumor detection, providing novel strategies for TNBC diagnosis.^{16,17}

A homing peptide-based active targeting system is an effective approach for delivering payloads such as imaging agents or drugs to diseased tissues.^{18,19} An increasing number of homing peptides for the diagnosis and treatment of tumors have been explored, such as iRGD, LyP-1, PL3, and Angiopep-2.^{19–21}

^a Department of Nuclear Medicine, Shanghai General Hospital, Shanghai Jiao Tong University School of Medicine, Shanghai 200080, P. R. China. E-mail: zhaojinhua1963@126.com

^b Academy of Chinese Medicine Sciences, Henan University of Chinese Medicine, Zhengzhou 450046, Henan, P. R. China

^c Department of Nuclear Medicine, General Hospital of Ningxia Medical University, Yinchuan 750004, Ningxia, P. R. China. E-mail: qin-yj06@163.com

^d School of Basic Medical Sciences, Ningxia Medical University, Yinchuan 750004, Ningxia, P. R. China. E-mail: jay70281@163.com

Among them, the heptapeptide A7R (ATWLPPR) screened by phage display technology has high affinity and specificity for VEGFR2 and NRP-1.^{22–24} Considering the overexpression of NRP-1 and VEGFR2 in various tumors, A7R has been used as a targeting ligand to construct imaging probes and targeted delivery systems for tumor imaging and therapy.^{24–27} Meanwhile, D-peptides that consist solely of D-amino acids possess unique advantages, including higher proteolytic stability and lower immunogenicity than L-peptides, and are emerging as a promising strategy in the field of cancer imaging and therapy.^{28,29} Recently, the D-type A7R peptide (^DA7R, ^DR^DP^DP^DL^DW^DT^DA) has also been shown to be an effective ligand owing to its enhanced targeting ability and stability compared to A7R.^{30–35} However, significant studies on radiolabeled A7R and ^DA7R are still insufficient.

In this study, [^{99m}Tc]Tc-labeled A7R and ^DA7R were designed and manufactured to develop novel single-photon emission computed tomography (SPECT) probes for TNBC imaging. To evaluate the targeting capacity in TNBC cells, A7R and ^DA7R were modified with fluorescein isothiocyanate (FITC) to form A7R-FITC and ^DA7R-FITC for flow cytometry and confocal microscopy *in vitro* and *ex vivo* fluorescence imaging. To label the heptapeptides with [^{99m}Tc]Tc in a simple procedure, their N-termini were conjugated with the commonly used bifunctional chelator 6-hydrazinonicotinic acid (HYNIC) to synthesize HYNIC-A7R and HYNIC-^DA7R (Fig. 1), respectively. The radiolabeled peptides were characterized by radio-high-performance liquid chromatography (radio-HPLC), and their radiochemical purities (RCPs) and stabilities *in vitro* in different media were tested by instant thin-layer chromatography (TLC). The imaging performance and biodistribution of [^{99m}Tc]Tc-HYNIC-A7R and [^{99m}Tc]Tc-HYNIC-^DA7R were confirmed in TNBC tumor-bearing mice. The data of this study demonstrated that both [^{99m}Tc]Tc-HYNIC-A7R and [^{99m}Tc]Tc-HYNIC-^DA7R could be readily prepared with high RCPs and stabilities, and showed obvious tumor accumulation with favorable biodistribution in 4T1 tumor-bearing mice,

suggesting their significant potential as probes for targeted SPECT imaging of TNBC. More importantly, [^{99m}Tc]Tc-HYNIC-^DA7R showed better tumor-to-muscle (T/M) ratios and lower renal uptake than [^{99m}Tc]Tc-HYNIC-A7R, which has distinct advantages for further clinical translation.

Experimental

Materials, cells and animal models

HYNIC-A7R, HYNIC-^DA7R, A7R-FITC, and ^DA7R-FITC were manufactured by ChinaPeptides Co. Ltd (Shanghai, China). Na[^{99m}Tc]TcO₄ was purchased from the Shanghai Atom Kexing Pharmaceutical Co., Ltd (Shanghai, China). CCK-8, RPMI-1640, FBS, 4',6-diamidino-2-phenylindole (DAPI), tris-buffered saline with Tween 20 (TBST), and TLC plates were supplied by Shanghai Dobio Co., Ltd (Shanghai, China). PBS, tricine, EDDA, SnCl₂ and cysteine were purchased from Shanghai Macklin Biochemical Co., Ltd (Shanghai, China). Other chemicals and solvents were supplied by Sinopharm Chemical Reagent Co., Ltd (Shanghai, China).

MCF-7 and 4T1 cells were supplied by Procell Life Science & Technology Co., Ltd (Wuhan, China) and maintained in RPMI-1640 supplemented with 10% FBS. Four-week-old female BALB/c nude mice (18–20 g) and healthy ICR mice (20–22 g) were purchased from the Shanghai Laboratory Animal Center of the Chinese Academy of Sciences (Shanghai, China). MCF-7 tumor-bearing mice were obtained from Cyagen Biosciences (Suzhou, China), and the 4T1-bearing mouse model was established as previously described.³⁹ Mice were used for animal experiments when the tumor diameter was 0.8–1.2 cm. All animal procedures were performed in accordance with the Guidelines for Care and Use of Laboratory Animals of Shanghai Jiao Tong University and approved by the Animal Ethics Committee of Shanghai General Hospital, Shanghai Jiao Tong University School of Medicine.

In vitro cytotoxicity assay

To assess the potential cytotoxicity of A7R and ^DA7R, cell viability was assessed using a CCK-8 assay. Briefly, 4T1 cells (1 × 10⁴ per well) were seeded into 96 well plates in RPMI-1640 with 10% FBS. After 24 h, the medium was replaced with 100 μL of fresh medium containing different concentrations of A7R or ^DA7R (0, 1, 5, 10, 20, 50, 100, and 200 μM). After 24 h, 10 μL of CCK-8 was added to the cells, and absorbance was measured after 1 h at 450 nm using a Varioskan Flash multimode microplate reader (Thermo Fisher Scientific, Waltham, MA, USA).

Immunoblotting analysis

NRP-1 expression in 4T1 and MCF-7 cells was confirmed using western blotting. Briefly, total protein was extracted from 4T1 and MCF-7 cells using RIPA buffer supplemented with phenylmethanesulfonyl fluoride, and debris was removed by centrifugation at 15 000 rpm for 10 min at 4 °C. The protein concentration was quantified using a bicinchoninic acid protein assay kit (Thermo Fisher Scientific, Waltham, MA, USA).

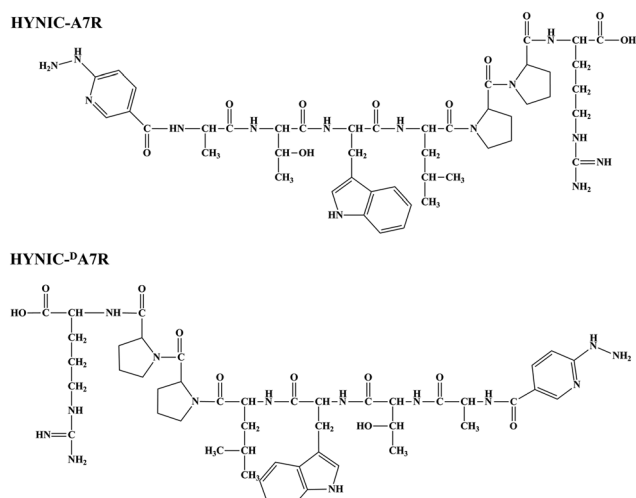


Fig. 1 Chemical structures of HYNIC-A7R and HYNIC-^DA7R.

The lysates were separated on sodium dodecyl sulfate-polyacrylamide gels and electrophoretically applied to polyvinylidene difluoride membranes. After blocking with 5% nonfat milk in TBST at 37 °C for 2 h, the membranes were incubated overnight with primary antibodies at a concentration of 1 : 1000 (anti-NRP-1 antibody and GAPDH were used as endogenous controls), followed by incubation with alkaline phosphatase-conjugated secondary antibodies at a concentration of 1 : 1000 for 2 h at room temperature in the dark. After washing in TBST, the protein bands were visualized using ECL. The blots were quantified using the ImageJ software (National Institutes of Health, Bethesda, MD, USA).

Flow cytometry and confocal microscopy

The specificity of A7R and ^DA7R for 4T1 cells was determined using flow cytometry. Briefly, 4T1 cells were seeded into 6 well plates at a density of 2×10^5 cells per well in 2 mL medium and cultured at 37 °C for 24 h. The cells were washed twice with PBS and incubated with 1 mL of fresh serum-free medium containing 10 μM A7R-FITC or ^DA7R-FITC. Cells treated with an equal volume of PBS were used as blank controls. After 2 h, cells were trypsinized and centrifuged at 1000 rpm for 3 min, washed, and resuspended in 1 mL PBS. FITC-positive cells were analyzed in the FL1-fluorescence channel using a BD Accuri™ C6 flow cytometer (BD Biosciences, Franklin Lakes, NJ, USA). At least 10 000 events were recorded for each sample.

The targeting abilities of A7R and ^DA7R for 4T1 cells were assessed using confocal microscopy. Briefly, 4T1 cells (2×10^5 cells) were seeded into glass-bottom dishes in 1 mL of medium. After 24 h, the medium was replaced with 2 mL of serum-free medium containing 10 μM A7R-FITC or ^DA7R-FITC. Cells treated with an equal volume of PBS were used as blank controls. After 2 h, the cells were rinsed three times with PBS, fixed with 4% paraformaldehyde in PBS for 15 min, and stained for nucleic acids with 200 μL of 1 μg mL⁻¹ DAPI for 5 min. After washing with PBS, fluorescence was analyzed using a Leica SP8 laser confocal microscope (Wetzlar, Germany).

Ex vivo fluorescence imaging

Fluorescence imaging was performed to test the *in vivo* targeting ability of A7R and ^DA7R. 4T1 tumor-bearing mice were randomly divided into two groups (three mice per group). After anesthetization with pentobarbital sodium (40 mg kg⁻¹), 200 μL solution of A7R-FITC or ^DA7R-FITC (1 mg mL⁻¹) was injected into the tail vein. The mice were euthanized 2 h post-injection to collect the tumors and major organs for *ex vivo* fluorescence imaging using an IVIS imaging system (IVIS Lumina Series III, PerkinElmer, Waltham, MA, USA), and the fluorescence intensities of tumors were quantified.

Radiolabeling and quality control

[^{99m}Tc]Tc-HYNIC-A7R and [^{99m}Tc]Tc-HYNIC-^DA7R were prepared as previously described.³⁷ Briefly, 50 μL of HYNIC-A7R or HYNIC-^DA7R solution (1 mg mL⁻¹ in water), 0.5 mL EDDA solution (20 mg mL⁻¹ in 0.1 M NaOH), 0.5 mL tricine solution (40 mg mL⁻¹ in 0.2 M PBS, pH = 6.0), 1 mL Na[^{99m}Tc]TcO₄

solution (50 mCi mL⁻¹), and 50 μL SnCl₂ solution (1 mg mL⁻¹ in 0.1 M HCl) were mixed and incubated at 100 °C. After 15 min, the reaction solution was cooled to room temperature and characterized using radio-HPLC. An H₂O and CH₃CN mixture containing 0.1% trifluoroacetic acid was used as the mobile phase at a flow rate of 1 mL min⁻¹, followed by a gradient of 20–50% CH₃CN for 0–20 min. The RCPs of radiolabeled peptides were rapidly quantified on silica gel 60 F254 TLC plates using 50% CH₃CN as the mobile phase. For the stability assessment *in vitro*, the [^{99m}Tc]Tc-labeled peptides were mixed with PBS or cysteine solution (100-fold molar excess over the peptides) at room temperature or FBS at 37 °C for 6 h. The RCPs were measured at different time points using the TLC method described above.

Partition coefficient measurement

Fifty microliter of the [^{99m}Tc]Tc-labeled peptides were mixed with 450 μL of PBS and 500 μL of *n*-octanol in 2 mL centrifuge tubes at room temperature. After 3 min of shaking, the mixtures were centrifuged at 5000 rpm for 5 min, and 50 μL of aliquot from the *n*-octanol and PBS were respectively collected to measure the radioactivity. The partition coefficient (*P*) was calculated by counts per minute in *n*-octanol/counts per minute in PBS. Measurements were conducted in parallel 5 times. Partition coefficient values were expressed as log *P* ± standard deviation.

In vivo SPECT imaging and immunohistochemical analysis

Ten 4T1 tumor-bearing mice were randomly divided into two groups (five mice per group). After anesthetization with pentobarbital sodium (40 mg kg⁻¹), they were injected with 200 μL of [^{99m}Tc]Tc-HYNIC-A7R or [^{99m}Tc]Tc-HYNIC-^DA7R ([^{99m}Tc]Tc = 10 mCi mL⁻¹) *via* the tail vein. SPECT images were acquired at 0.5, 1, 2, and 4 h post-injection using the GE Infinia SPECT scanner (Denver, CO, USA). To assess the specificities of the [^{99m}Tc]Tc-labeled peptides, blocking studies were performed using another ten 4T1 tumor-bearing mice. The blocking agents A7R and ^DA7R (approximately 500 μg per mouse) were co-injected with [^{99m}Tc]Tc-HYNIC-A7R or [^{99m}Tc]Tc-HYNIC-^DA7R at the same dosages, and SPECT images were acquired at the same time points.

After SPECT imaging, the tumors and muscle tissues were excised to analyze VEGFR2 and NRP-1 expression. Briefly, the excised samples were fixed in formalin, embedded in paraffin, cut into 5 μm sections, stained with hematoxylin solution for 5 min, and stained with eosin solution for 3 min. Tumor sections were incubated further with antibodies against NRP-1 (1 : 100) or VEGFR2 (1 : 50) at 4 °C overnight. After washing three times with PBS, the sections were incubated with a secondary antibody (1 : 200) for 50 min. After three PBS washes, the slides were stained with a freshly prepared DAB solution to terminate the color reaction. The slides were counterstained with Harris hematoxylin for approximately 3 min, washed with ammonia, and rinsed with running water. Slides were dehydrated in an alcohol gradient, mounted, and then imaged and analyzed.

Biodistribution and pharmacokinetics

Mice were intravenously injected with 200 μL [$^{99\text{m}}\text{Tc}$]Tc-HYNIC-A7R or [$^{99\text{m}}\text{Tc}$]Tc-HYNIC- $^{\text{D}}$ A7R ([$^{99\text{m}}\text{Tc}$]Tc = 100 $\mu\text{Ci mL}^{-1}$) to determine their biodistribution properties. Mice were sacrificed by cervical dislocation at 0.5, 1, 2, or 4 h after injection. The tumors and major organs, including the liver, spleen, kidneys, heart, lung, stomach, intestines, and muscle, were collected and weighed. The radioactivity counts of all the samples were measured using a γ -counter (CAPINTEC, USA). The results are shown as the percentage of injection dose per gram (%ID g^{-1}) of wet tissue.

The pharmacokinetics of [$^{99\text{m}}\text{Tc}$]Tc-HYNIC-A7R and [$^{99\text{m}}\text{Tc}$]Tc-HYNIC- $^{\text{D}}$ A7R were determined in healthy ICR mice. Mice were randomly divided into nine groups ($n = 3$), and each mouse received a dose of 200 μL [$^{99\text{m}}\text{Tc}$]Tc-HYNIC-A7R or [$^{99\text{m}}\text{Tc}$]Tc-HYNIC- $^{\text{D}}$ A7R ([$^{99\text{m}}\text{Tc}$]Tc = 100 $\mu\text{Ci mL}^{-1}$). At designated times (1, 5, 10, 15, 30, 60, 120, 240, and 360 min), 100 μL blood was immediately collected and weighed. The radioactivity counts of the blood samples were measured using the γ -counter to calculate the %ID g^{-1} . Pharmacokinetic data were analyzed using DAS 2.0 (Shanghai, China), and the half-lives of [$^{99\text{m}}\text{Tc}$]Tc-HYNIC-A7R and [$^{99\text{m}}\text{Tc}$]Tc-HYNIC- $^{\text{D}}$ A7R in the blood were calculated using a two-compartment model.

Statistical analysis

Data are presented as mean \pm standard deviation. The significance of the data was analyzed using one-way analysis of variance with $p < 0.05$ as the threshold of significance. The data are described as follows: * < 0.05 , ** < 0.01 , and *** < 0.001 , respectively.

Results and discussion

Cytotoxicity and NRP-1 expression in tumor cells

The potential cytotoxic effects of A7R-HYNIC and $^{\text{D}}$ A7R-HYNIC in 4T1 cells were determined using cell counting kit-8 (CCK-8) assays. After incubation at the concentration range of 0–200 μM for 24 h, cells treated with all concentrations of A7R-HYNIC and $^{\text{D}}$ A7R-HYNIC were more than 90% viable (Fig. 2A), suggesting good cytocompatibility *in vitro*. The expression of NRP-1 in 4T1 cells was analyzed using immunoblotting, and MCF-7 cells were used as a negative control. The results showed high expression of NRP-1 in 4T1 cells compared to that in MCF-7 cells, suggesting high NRP-1 expression in TNBC cells (Fig. 2B), which is in accordance with the literature.³⁶ Quantitative analysis further revealed that the level of NRP-1 in 4T1 cells was significantly higher than that in MCF-7 cells (Fig. 2C).

Targeting abilities of A7R and $^{\text{D}}$ A7R to 4T1 cells *in vitro*

The targeting abilities of A7R-FITC and $^{\text{D}}$ A7R-FITC to 4T1 cells were confirmed and compared using flow cytometry and confocal microscopy. As shown in Fig. 3A–C, the fluorescence intensities of 4T1 cells treated with A7R-FITC and $^{\text{D}}$ A7R-FITC were stronger than those of the cells treated with PBS after 3 h, indicating good targeting abilities *in vitro*. Moreover, a

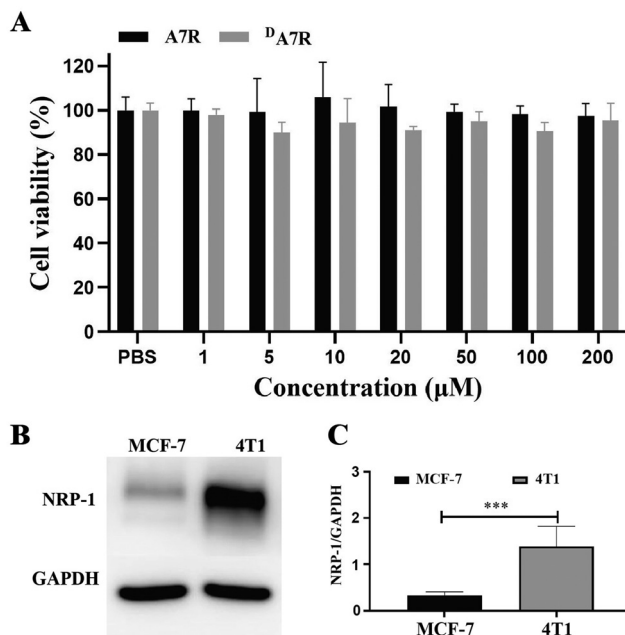


Fig. 2 Excellent cytocompatibilities of A7R and $^{\text{D}}$ A7R *in vitro* and high expression of NRP-1 in 4T1 cells. (A) Viability of 4T1 cells treated with 0 to 200 μM A7R-HYNIC or $^{\text{D}}$ A7R-HYNIC for 24 h. (B) Western blot results and (C) quantitative analysis of NRP-1 expression in 4T1 and MCF-7 cells.

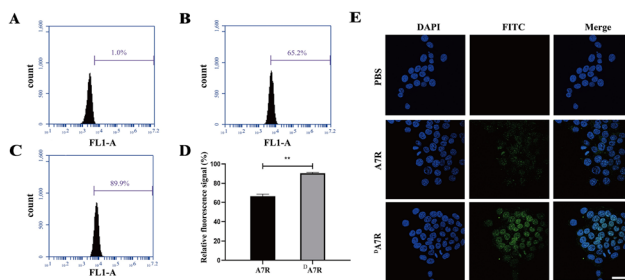


Fig. 3 High targeting abilities *in vitro* of A7R-FITC and $^{\text{D}}$ A7R-FITC. The 4T1 cells were treated with (A) PBS, (B) 10 μM A7R-FITC, or (C) $^{\text{D}}$ A7R-FITC for 3 h. (D) Quantitative analysis of A7R-FITC and $^{\text{D}}$ A7R-FITC in 4T1 cells. (E) Confocal microscopy images of 4T1 cells treated with 10 μM A7R-FITC or $^{\text{D}}$ A7R-FITC for 3 h. The scale bar represents 200 μm for all panels.

significantly higher fluorescence intensity was observed in 4T1 cells treated with $^{\text{D}}$ A7R-FITC, suggesting its better targeting capacity than A7R-FITC (Fig. 3D). Fluorescence signals were also observed in 4T1 cells treated with $^{\text{D}}$ A7R-FITC and A7R-FITC using confocal microscopy, with the strongest signal occurring in the cells treated with $^{\text{D}}$ A7R-FITC. However, no fluorescence signal was found in cells treated with PBS (Fig. 3E). These data further support that the A7R and $^{\text{D}}$ A7R peptides can bind to 4T1 cells and that $^{\text{D}}$ A7R has a better targeting ability than A7R *in vitro*.

Ex vivo fluorescence imaging

To investigate their tumor-targeting abilities *in vivo*, A7R-FITC and $^{\text{D}}$ A7R-FITC were intravenously injected into 4T1 tumor-bearing

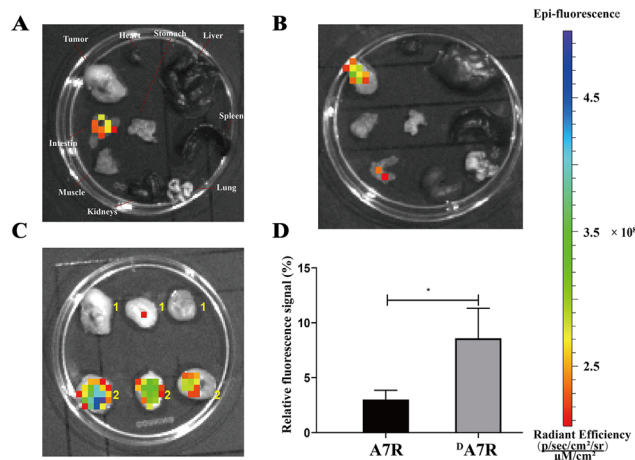


Fig. 4 Obvious accumulation of $^{\text{D}}\text{A7R-FITC}$ and A7R-FITC in 4T1 tumors. *Ex vivo* fluorescence imaging of 4T1 tumors at 2 h after intravenous injection of (A) A7R-FITC and (B) $^{\text{D}}\text{A7R-FITC}$. (C) *Ex vivo* tumor fluorescence imaging and (D) quantitative analysis of A7R-FITC (up) and $^{\text{D}}\text{A7R-FITC}$ (down) at 2 h post-injection.

nude mice, and the tumors and major organs were collected at 2 h post-injection for *ex vivo* fluorescence imaging. As shown in Fig. 4A and B, both A7R-FITC and $^{\text{D}}\text{A7R-FITC}$ showed preferential accumulation in the tumors and low accumulation in the major organs, such as the liver, kidneys, stomach, heart, and lungs. This high tumor accumulation was beneficial for distinguishing tumors from surrounding tissues, indicating the good targeting abilities of A7R and $^{\text{D}}\text{A7R}$ for *in vivo* imaging of TNBC. Moreover, tumors from mice treated with $^{\text{D}}\text{A7R-FITC}$ had higher tumor fluorescence intensities than those from mice treated with A7R-FITC under the same conditions (Fig. 4C and D), which was consistent with the higher fluorescence intensity associated with $^{\text{D}}\text{A7R-FITC}$ *in vitro*, further supporting the superior specificity of $^{\text{D}}\text{A7R}$. It should be noted that D-type peptides have higher stability *in vivo*, such as resistance to endogenous enzymes, which may be the reason for the better tumor accumulation of $^{\text{D}}\text{A7R-FITC}$ compared to A7R-FITC .^{30,33}

Radiolabeling and quality control

$^{99\text{m}}\text{Tc}$ is a prior choice for SPECT imaging due to its intrinsic advantages such as appropriate half-life (6.02 h) and low energy γ -ray (140 keV). To conveniently label peptides with $^{99\text{m}}\text{Tc}$ and form stable probes for tumor imaging, the selection of suitable bifunctional chelator is of importance. HYNIC is one of the most commonly used bifunctional chelators in technetium chemistry because of its easy modification and high labeling efficiency. In our previous study, we reported a $^{99\text{m}}\text{Tc}$ -labeled HYNIC-modified heptapeptide with high RCP and excellent stability, which exhibited favorable accumulation in several types of tumors.³⁷ Therefore, we used HYNIC to modify A7R and $^{\text{D}}\text{A7R}$ peptides, which were then readily labeled with $^{99\text{m}}\text{Tc}$ using tricine and ethylenediamine-*N,N'*-diacetic acid (EDDA) as co-ligands according to the literature.³⁸

The prepared $^{99\text{m}}\text{Tc}$ -HYNIC- A7R and $^{99\text{m}}\text{Tc}$ -HYNIC- $^{\text{D}}\text{A7R}$ were characterized using radio-HPLC. As shown in Fig. 5A and B, a

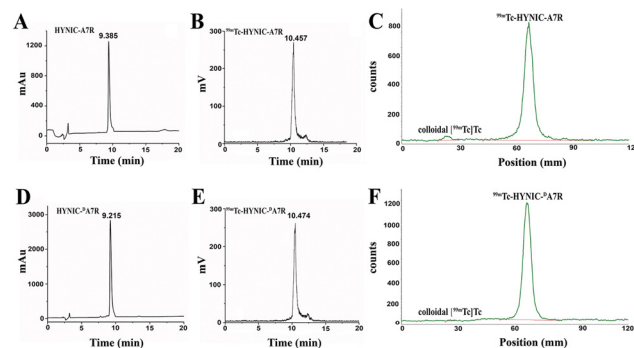


Fig. 5 RCPs of $^{99\text{m}}\text{Tc}$ -labeled peptides. Radio-HPLC and TLC results of (A–C) $^{99\text{m}}\text{Tc}$ -HYNIC- A7R and (D–F) $^{99\text{m}}\text{Tc}$ -HYNIC- $^{\text{D}}\text{A7R}$.

single radioactive peak of $^{99\text{m}}\text{Tc}$ -HYNIC- A7R was observed at a retention time of 10.457 min, corresponding to HYNIC- A7R (9.385 min). Similar results were observed for $^{99\text{m}}\text{Tc}$ -HYNIC- $^{\text{D}}\text{A7R}$ (10.474 min, Fig. 5D) and HYNIC- $^{\text{D}}\text{A7R}$ (9.215 min, Fig. 5E). These results proved the success of radiolabeling, and the RCPs of these $^{99\text{m}}\text{Tc}$ -labeled peptides were calculated to be more than 95% with a specific radioactivity of 1000 Ci g^{-1} ; therefore, there was no need for further purification. The RCPs of $^{99\text{m}}\text{Tc}$ -labeled peptides can be rapidly estimated using the TLC method reported in the literature.³⁷ As shown in Fig. 5C and F, after performing the reaction mixture by TLC plates using methanol containing 1% HCl as the mobile phase, single peaks of $^{99\text{m}}\text{Tc}$ -HYNIC- A7R and $^{99\text{m}}\text{Tc}$ -HYNIC- $^{\text{D}}\text{A7R}$ were observed with a retention factor of 0.5, whereas the retention factors of colloidal $^{99\text{m}}\text{Tc}$ and unreacted $\text{Na}^{99\text{m}}\text{TcO}_4$ were 0 and 1, respectively. Using the same TLC method, the stabilities of $^{99\text{m}}\text{Tc}$ -HYNIC- A7R and $^{99\text{m}}\text{Tc}$ -HYNIC- $^{\text{D}}\text{A7R}$ were tested in fetal bovine serum (FBS) at 37°C and PBS and cysteine solution (100-fold molar excess of peptides) at room temperature. As we anticipated, no significant decreases in the RCPs were observed within 6 h under these conditions, suggesting the high stability of $^{99\text{m}}\text{Tc}$ -HYNIC- A7R and $^{99\text{m}}\text{Tc}$ -HYNIC- $^{\text{D}}\text{A7R}$ *in vitro*. Moreover, the partition coefficient values of $^{99\text{m}}\text{Tc}$ -HYNIC- A7R and $^{99\text{m}}\text{Tc}$ -HYNIC- $^{\text{D}}\text{A7R}$ were -2.06 ± 0.04 and -2.16 ± 0.13 , respectively. The data revealed the similar hydrophilicity of the formed probes.

In vivo SPECT imaging and biodistribution

A7R and $^{\text{D}}\text{A7R}$ have been used as targeting ligands in a variety of tumor-targeted imaging probes and delivery systems.^{24–27,30–35} The good targeting abilities of A7R and $^{\text{D}}\text{A7R}$ for VEGFR2 and NRP-1 also arouse the interest of researchers in the field of radiopharmaceuticals. In a previous study, A7R was successfully labeled with $^{99\text{m}}\text{Tc}$ using a benzoyl mercaptoacetyl group and showed high affinity to NRP-1 *in vitro*.³⁸ However, this radiolabeled compound displayed an obvious uptake by the digestive tract rather than the tumor region in a TNBC model. In a recent study, ^{68}Ga and ^{177}Lu labeled A7R were prepared with high radiochemical purity and satisfactory stability *in vitro*, but no biological tests at the cellular or animal levels were reported.²⁶ Thus, the

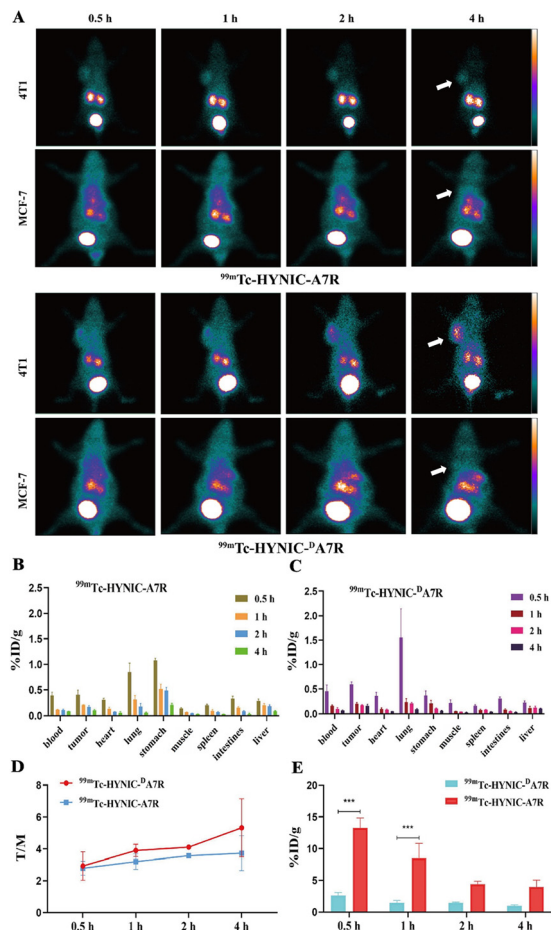


Fig. 6 Favorable SPECT imaging and biodistribution of [^{99m}Tc]Tc-labeled peptides. (A) SPECT images of 4T1 and MCF-7 tumor-bearing mice at different time points after injection with [^{99m}Tc]Tc-HYNIC-A7R and [^{99m}Tc]Tc-HYNIC- $^{\text{D}}$ A7R. White arrows represent the tumors. Biodistribution of (B) [^{99m}Tc]Tc-HYNIC-A7R and (C) [^{99m}Tc]Tc-HYNIC- $^{\text{D}}$ A7R in 4T1 tumor-bearing mice. (D) Tumor-to-muscle (T/M) ratios and (E) comparison of renal uptake of [^{99m}Tc]Tc-HYNIC-A7R and [^{99m}Tc]Tc-HYNIC- $^{\text{D}}$ A7R at different time points.

studies on radiolabeled A7R and $^{\text{D}}$ A7R are still inadequate, and their significant values need to be further examined.

To evaluate the feasibility of [^{99m}Tc]Tc-HYNIC-A7R and [^{99m}Tc]Tc-HYNIC- $^{\text{D}}$ A7R for imaging of TNBCs *in vivo*, we intravenously injected the formed probes into 4T1 tumor-bearing nude mice. Mice with MCF-7 tumors were used as controls. As shown in Fig. 6A, both 4T1 and MCF-7 tumor-bearing mice treated with [^{99m}Tc]Tc-HYNIC-A7R and [^{99m}Tc]Tc-HYNIC- $^{\text{D}}$ A7R displayed high radioactivity in the kidneys and bladder at each time point, whereas obvious SPECT signals in tumors occurred only in the 4T1 tumor-bearing mice. Remarkably, the tumors were clearly visible at 0.5 h post-injection in the mice injected with [^{99m}Tc]Tc-HYNIC- $^{\text{D}}$ A7R and [^{99m}Tc]Tc-HYNIC-A7R, indicating that [^{99m}Tc]Tc-labeled A7R and $^{\text{D}}$ A7R peptides could be used as SPECT probes for TNBC imaging. In line with our *in vitro* and *ex vivo* results, an increased trend of tumor SPECT signal intensity over time was observed in mice injected with [^{99m}Tc]Tc-HYNIC- $^{\text{D}}$ A7R, whereas no significant changes were

observed in mice injected with [^{99m}Tc]Tc-HYNIC-A7R over the imaging time course, suggesting that $^{\text{D}}$ A7R had better imaging performance *in vivo*.

The SPECT imaging findings were further verified using biodistribution experiments. As shown in Fig. 6B and C, the tumor accumulation of [^{99m}Tc]Tc-HYNIC- $^{\text{D}}$ A7R was $0.60 \pm 0.05\% \text{ID g}^{-1}$ at 0.5 h post-injection, which was higher than that of [^{99m}Tc]Tc-HYNIC-A7R ($0.39 \pm 0.09\% \text{ID g}^{-1}$) at the same time point. Despite elimination with time, [^{99m}Tc]Tc-HYNIC- $^{\text{D}}$ A7R still had a better tumor uptake than [^{99m}Tc]Tc-HYNIC-A7R ($0.16 \pm 0.03\% \text{ID g}^{-1}$ vs. $0.10 \pm 0.02\% \text{ID g}^{-1}$) at 4 h post-injection. In addition, [^{99m}Tc]Tc-HYNIC- $^{\text{D}}$ A7R had higher T/M ratios than [^{99m}Tc]Tc-HYNIC-A7R at each time point, supporting its better imaging performance (Fig. 6D). Notably, although the kidneys had the highest uptake of [^{99m}Tc]Tc-HYNIC-A7R and [^{99m}Tc]Tc-HYNIC- $^{\text{D}}$ A7R, there was a significant difference between them. As shown in Fig. 6E, the kidney uptake of [^{99m}Tc]Tc-HYNIC-A7R was up to $13.27 \pm 1.55\% \text{ID g}^{-1}$ at 0.5 h post-injection, whereas that of [^{99m}Tc]Tc-HYNIC- $^{\text{D}}$ A7R was only $2.59 \pm 4.89\% \text{ID g}^{-1}$. A significantly lower renal uptake of the D-type peptide was also observed at all other time points, indicating its low retention in the kidneys and fast clearance from the urinary system. This may be involved with multiple aspects of the $^{\text{D}}$ -peptide, including its stability and negative charge.⁴⁰ The exact mechanism is unclear, and further experiments are warranted. To further verify the specificities of [^{99m}Tc]Tc-labeled peptides, blocking experiments were performed *in vivo*. As shown in Fig. 7, the tumor uptake of [^{99m}Tc]Tc-HYNIC-A7R and [^{99m}Tc]Tc-HYNIC- $^{\text{D}}$ A7R was obviously inhibited by co-injection of unlabeled peptides at each time point, demonstrating the specificities of the probes.

Immunohistochemistry

After SPECT imaging, the NRP-1 and VEGFR2 expression in tumor tissues was evaluated using immunohistochemistry in mice injected with [^{99m}Tc]Tc-HYNIC-A7R and [^{99m}Tc]Tc-HYNIC- $^{\text{D}}$ A7R. Normal muscle tissues were used as negative controls. As shown in Fig. 8, the levels of NRP-1 and VEGFR2 in 4T1 tumors were higher than those in MCF-7 tumors, and no

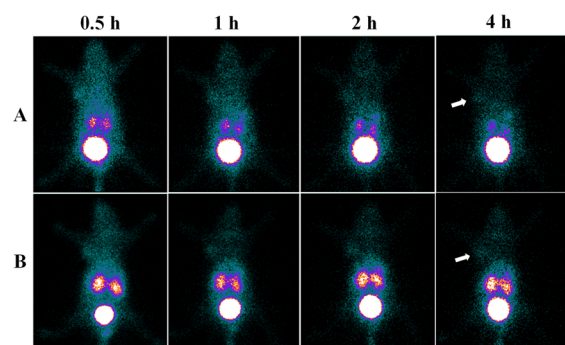


Fig. 7 Blocking experiments of (A) [^{99m}Tc]Tc-HYNIC-A7R and (B) [^{99m}Tc]Tc-HYNIC- $^{\text{D}}$ A7R in 4T1 xenograft mice at different time points. White arrows represent the tumors.

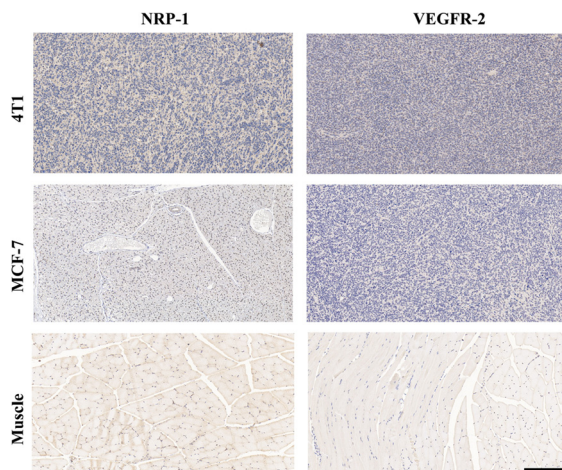


Fig. 8 Immunohistochemistry images of VEGFR2 and NRP-1 in 4T1 and MCF-7 tumors and muscle (control). The scale bar represents 200 μm for all panels.

obvious NRP-1 or VEGFR2 expression was observed in the muscle. These data correlated well with SPECT imaging results and further validated the specificity of $[^{99\text{m}}\text{Tc}]$ Tc-HYNIC-A7R and $[^{99\text{m}}\text{Tc}]$ Tc-HYNIC- $^{\text{D}}$ A7R for TNBC imaging *in vivo*.

Pharmacokinetics

The radioactivity–time curves of the $[^{99\text{m}}\text{Tc}]$ Tc-labeled peptides are shown in Fig. 9. A fast blood clearance was observed within 30 min after injection. The initial radioactivities of $[^{99\text{m}}\text{Tc}]$ Tc-HYNIC-A7R and $[^{99\text{m}}\text{Tc}]$ Tc-HYNIC- $^{\text{D}}$ A7R in the blood at 1 min post-injection were $19.21 \pm 1.72\% \text{ID g}^{-1}$ and $15.93 \pm 2.61\% \text{ID g}^{-1}$, respectively, and they rapidly decreased to $1.31 \pm 0.11\% \text{ID g}^{-1}$ and $1.23 \pm 0.19\% \text{ID g}^{-1}$ at 30 min post-injection, respectively. Both of them showed radioactivities of less than $0.1\% \text{ID g}^{-1}$ after 240 min. The distribution phase half-lives of $[^{99\text{m}}\text{Tc}]$ Tc-HYNIC-A7R and $[^{99\text{m}}\text{Tc}]$ Tc-HYNIC- $^{\text{D}}$ A7R were 0.464 and 2.477 min, respectively, and their clearance phase half-lives were 7.281 and 13.678 min, respectively. This rapid blood clearance is not only favorable for imaging tumors at an early time point but also reduces nonspecific uptake in normal tissues, which further improves the contrast of tumors.

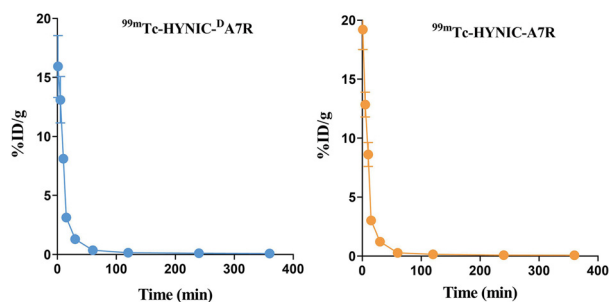


Fig. 9 Radioactivity–time curves of $[^{99\text{m}}\text{Tc}]$ Tc-HYNIC- $^{\text{D}}$ A7R and $[^{99\text{m}}\text{Tc}]$ Tc-HYNIC-A7R in ICR mice.

Conclusions

In this study, we designed and prepared $[^{99\text{m}}\text{Tc}]$ Tc-labeled A7R and $^{\text{D}}$ A7R as SPECT probes for TNBC imaging. A7R and $^{\text{D}}$ A7R were easily labeled with $[^{99\text{m}}\text{Tc}]$ Tc through HYNIC. Both the $[^{99\text{m}}\text{Tc}]$ Tc-HYNIC-A7R and $[^{99\text{m}}\text{Tc}]$ Tc-HYNIC- $^{\text{D}}$ A7R had high RCPs and stabilities *in vitro* and showed obvious tumor accumulation in TNBC-bearing mice with favorable biodistribution and fast blood clearance, indicating significant potential for targeted SPECT imaging of TNBC. Furthermore, $[^{99\text{m}}\text{Tc}]$ Tc-HYNIC- $^{\text{D}}$ A7R showed better T/M ratios and lower renal uptake than $[^{99\text{m}}\text{Tc}]$ Tc-HYNIC-A7R; therefore, it should be considered for future clinical translation.

Author contributions

Hongxing Su, Lingzhou Zhao, and Buhui Yu equally contributed to this work.

Conflicts of interest

There are no conflicts to declare.

Acknowledgements

This research was funded by the Ningxia Key Research and Development Program (2020BFG03005 and 2019BEG03018), the Ningxia Natural Science Foundation (2022AAC03136) and the National Natural Science Foundation of China (81971647 and 8197070412).

References

- H. Sung, J. Ferlay, R. L. Siegel, M. Laversanne, I. Soerjomataram, A. Jemal and F. Bray, *Ca-Cancer J. Clin.*, 2021, **71**, 209–249.
- L. Yin, J. J. Duan, X. W. Bian and S. C. Yu, *Breast Cancer Res.*, 2020, **22**, 61.
- D. D. Singh and D. K. Yadav, *Biomedicines*, 2021, **9**, 876.
- J. Y. S. Tsang and G. M. Tse, *Adv. Anat. Pathol.*, 2020, **27**, 27–35.
- A. C. Garrido-Castro, N. U. Lin and K. Polyak, *Cancer Discov.*, 2019, **9**, 176–198.
- C. Elfgen, Z. Varga, K. Reeve, L. Moskovszky, V. Bjelic-Radisic, C. Tausch and U. Güth, *Breast Cancer Res. Treat.*, 2019, **177**, 67–75.
- B. Shashni, Y. Nishikawa and Y. Nagasaki, *Biomaterials*, 2021, **269**, 120645.
- K. Masłowska, P. K. Halik, D. Tymecka, A. Misicka and E. Gniazdowska, *Cancers*, 2021, **13**, 1072.
- H. F. Guo and C. W. Vander Kooi, *J. Biol. Chem.*, 2015, **290**, 29120–29126.
- M. Geindreau, F. Ghiringhelli and M. Bruchard, *Int. J. Mol. Sci.*, 2021, **22**, 4871.
- A. A. Shah, M. A. Kamal and S. Akhtar, *Curr. Drug Metab.*, 2021, **22**, 50–59.

- 12 R. Lugano, M. Ramachandran and A. Dimberg, *Cell. Mol. Life Sci.*, 2020, **77**, 1745–1770.
- 13 B. Chaudhary, Y. S. Khaled, B. J. Ammori and E. Elkord, *Cancer Immunol. Immunother.*, 2014, **63**, 81–99.
- 14 C. Hu and X. Jiang, *Target. Oncol.*, 2016, **11**, 501–505.
- 15 H. Wang, Y. N. Zhang, D. Q. Xu, J. G. Huang, D. Lv, X. Y. Shi, J. Y. Liu, H. W. Ren and Z. X. Han, *Neoplasma*, 2020, **67**, 1335–1342.
- 16 A. Moussaron, V. Jouan-Hureaux, C. Collet, J. Pierson, N. Thomas, L. Choulier, N. Veran, M. Doyen, P. Arnoux, F. Maskali, D. Dumas, S. Acherar, M. Barberi-Heyob and C. Frochot, *Molecules*, 2021, **26**, 7273.
- 17 B. Mitran, R. Güler, F. P. Roche, E. Lindström, R. K. Selvaraju, F. Fleetwood, S. S. Rinne, L. Claesson-Welsh, V. Tolmachev, S. Ståhl, A. Orlova and J. Löfblom, *Theranostics*, 2018, **8**, 4462–4476.
- 18 P. Lingasamy and T. Teesalu, *Adv. Exp. Med. Biol.*, 2021, **1295**, 29–48.
- 19 E. Kondo, H. Iioka and K. Saito, *Cancer Sci.*, 2021, **112**, 2118–2125.
- 20 K. N. Sugahara, G. B. Braun, T. H. de Mendoza, V. R. Kotamraju, R. P. French, A. M. Lowy, T. Teesalu and E. Ruoslahti, *Mol. Cancer Ther.*, 2015, **14**, 120–128.
- 21 P. Lingasamy, A. Tobi, K. Kurm, S. Kopanchuk, A. Sudakov, M. Salumäe, T. Rätsep, T. Asser, R. Bjerkvig and T. Teesalu, *Sci. Rep.*, 2020, **10**, 5809.
- 22 L. Tirand, C. Frochot, R. Vanderesse, N. Thomas, E. Trinquet, S. Pinel, M. L. Viriot, F. Guillemain and M. Barberi-Heyob, *J. Controlled Release*, 2006, **111**, 153–164.
- 23 R. Binétruy-Tournaire, C. Demangel, B. Malavaud, R. Vassy, S. Rouyre, M. Kraemer, J. Plouët, C. Derbin, G. Perret and J. C. Mazié, *EMBO J.*, 2000, **19**, 1525–1533.
- 24 L. Lu, H. Chen, D. Hao, X. Zhang and F. Wang, *Asian J. Pharm. Sci.*, 2019, **14**, 595–608.
- 25 J. Wu, D. H. Bremner, S. Niu, D. Li, R. Tang and L. M. Zhu, *J. Biomed. Nanotechnol.*, 2019, **15**, 1415–1431.
- 26 K. Masłowska, E. Witkowska, D. Tymecka, P. K. Halik, A. Misicka and E. Gniazdowska, *Pharmaceutics*, 2022, **14**, 100.
- 27 H. Wang, X. Wang, C. Xie, M. Zhang, H. Ruan, S. Wang, K. Jiang, F. Wang, C. Zhan, W. Lu and H. Wang, *J. Controlled Release*, 2018, **284**, 26–38.
- 28 J. Bastings, H. M. van Eijk, S. W. Olde Damink and S. S. Rensen, *Nutrients*, 2019, **11**, 2205.
- 29 K. Luyten, T. Van Loy, C. Cawthorne, C. M. Deroose, D. Schols, G. Bormans and F. Cleeren, *Pharmaceutics*, 2021, **13**, 1619.
- 30 M. Zhang and W. Lu, *Acta Pharm. Sin. B*, 2018, **8**, 106–115.
- 31 M. Ying, S. Wang, M. Zhang, R. Wang, H. Zhu, H. Ruan, D. Ran, Z. Chai, X. Wang and W. Lu, *ACS Appl. Mater. Interfaces*, 2018, **10**, 19473–19482.
- 32 M. Zhang, L. Lu, M. Ying, H. Ruan, X. Wang, H. Wang, Z. Chai, S. Wang, C. Zhan, J. Pan and W. Lu, *Mol. Pharm.*, 2018, **15**, 2437–2447.
- 33 M. Ying, Q. Shen, Y. Liu, Z. Yan, X. Wei, C. Zhan, J. Gao, C. Xie, B. Yao and W. Lu, *ACS Appl. Mater. Interfaces*, 2016, **8**, 13232–13241.
- 34 L. Cui, Y. Wang, M. Liang, X. Chu, S. Fu, C. Gao, Q. Liu, W. Gong, M. Yang, Z. Li, L. Yu, C. Yang, Z. Su, X. Xie, Y. Yang and C. Gao, *Drug Deliv.*, 2018, **25**, 1865–1876.
- 35 L. Jiao, Q. Dong, W. Zhai, W. Zhao, P. Shi, Y. Wu, X. Zhou and Y. Gao, *Pharmacol. Res.*, 2022, **182**, 106343.
- 36 J. Zhang, X. Zhang, Z. Li, Q. Wang, Y. Shi, X. Jiang and X. Sun, *Front. Oncol.*, 2021, **11**, 654672.
- 37 J. Gong, L. Zhao, J. Yang, M. Zhu and J. Zhao, *Pharmaceutics*, 2022, **14**, 996.
- 38 G. Y. Perret, A. Starzec, N. Hauet, J. Vergote, M. Le Pecheur, R. Vassy, G. Léger, K. A. Verbeke, G. Bormans, P. Nicolas, A. M. Verbruggen and J. L. Moretti, *Nucl. Med. Biol.*, 2004, **31**, 575–581.
- 39 N. Song, L. Zhao, X. Xu, M. Zhu, C. Liu, N. Sun, J. Yang, X. Shi and J. Zhao, *ACS Appl. Mater. Interfaces*, 2020, **12**, 12395–12406.
- 40 M. Gotthardt, J. van Eerd-Vismale, W. J. Oyen, M. de Jong, H. Zhang, E. Rolleman, H. R. Maecke, M. Béhé and O. Boerman, *J. Nucl. Med.*, 2007, **48**, 596–601.